



Strato-mesospheric carbon monoxide profiles above Kiruna, Sweden (67.8° N, 20.4° E), since 2008

Niall J. Ryan¹, Mathias Palm¹, Uwe Raffalski², Richard Larsson³, Gloria Manney⁴, Luis Millán⁵, and Justus Notholt¹

¹Institute of Environmental Physics, University of Bremen, 28359 Bremen, Germany

²Swedish Institute of Space Physics, Box 812, 981 28 Kiruna, Sweden

³National Institute of Information and Communications Technology, Tokyo, Japan

⁴NorthWest Research Associates, Socorro, New Mexico, USA and Department of Physics, New Mexico Institute of Mining and Technology, Socorro, NM 87801, USA

⁵Jet Propulsion Laboratory, M/S 183-701, 4800 Oak Grove Drive, Pasadena, CA 91109, USA

Correspondence to: Niall J. Ryan (n_ryan@iup.physik.uni-bremen.de)

Received: 22 August 2016 – Discussion started: 10 October 2016

Revised: 24 December 2016 – Accepted: 27 December 2016 – Published: 13 February 2017

Abstract. This paper presents the retrieval and validation of a self-consistent time series of carbon monoxide (CO) above Kiruna using measurements from the Kiruna Microwave Radiometer (KIMRA). The data set currently spans the years 2008–2015, and measurements are ongoing at Kiruna. The spectra are inverted using an optimal estimation method to retrieve altitude profiles of CO concentrations in the atmosphere within an average altitude range of 48–84 km. Atmospheric temperature data from the Special Sensor Microwave Imager/Sounder aboard the US Air Force meteorological satellite DMSP-F18, are used in the inversion of KIMRA spectra between January 2011 and May 2014. This KIMRA CO data set is compared with CO data from the Microwave Limb Sounder aboard the Aura satellite: there is a maximum bias for KIMRA of ~ 0.65 ppmv at 68 km (corresponding to 14.7 % of the mean CO value at 68 km) and a maximum relative bias of 22 % (0.44 ppmv) at 60 km. Standard deviations of the differences between profiles are similar in magnitude to the estimated uncertainties in the profiles. Correlations between the instruments are within 0.87 and 0.94. These numbers indicate agreement between the instruments. To expand the CO data set outside of the lifetime of DMSP-F18, another inversion setup was used that incorporates modelled temperatures from the European Centre for Medium-Range Weather Forecasts. The effect on the retrieved CO profiles when using a different temperature data set in the inversion was assessed. A comparison of the two overlapping KIMRA CO data sets shows a positive bias of $< 5\%$ in the extended data set and a correlation > 0.98 between the lower retrievable altitude limit and 82.5 km. The extended data set shows a larger range ($\leq 6\%$) of CO concentrations that is not explained by random error estimates. Measurements are continuing and the extended KIMRA CO time series currently spans 2008–2015, with gaps corresponding to non-operation and summer periods when CO concentrations below ~ 90 km drop to very low values.

The data can be accessed at doi:10.1594/PANGAEA.861730.

1 Introduction

The principle source of carbon monoxide (CO) in the middle atmosphere is the photolysis of carbon dioxide (CO₂) in the thermosphere and its subsequent vertical transport, and its only sink is through reaction with the hydroxyl radical (OH) (Solomon et al., 1985). The loss rates in the thermosphere are low and this leads to a strong vertical gradient in CO concentrations (volume mixing ratio (VMR) is the form of gas concentration used throughout this work, and the two terms are considered to be synonymous here). As the production and loss mechanisms for atmospheric CO require the presence of sunlight, the lifetime of CO during polar winter is on the order of months (Solomon et al., 1985; Allen et al., 1999), making it an excellent tracer for atmospheric dynamics. In spring the lifetime in the upper stratosphere can be 15–20 days poleward of 60° latitude (Minschwaner et al., 2010). Due to the longer CO lifetimes within the polar vortex during winter, there exists also a strong horizontal concentration gradient across the vortex boundary.

While satellite measurements of CO profiles have been used regularly to study atmospheric transport processes, particularly during northern winters (e.g. Damiani et al., 2014; Lee et al., 2011; Manney et al., 2009; McLandress et al., 2013), ground-based CO profile data sets for the poles are few and far between. The ground-based millimetre-wave spectrometer (GBMS) installed in Thule Air Base, Greenland (76.5° N, 68.7° W), was used to study the composition of the Arctic winter atmosphere in 2001/02 (Muscari et al., 2007) and the sudden stratospheric warming (SSW) of 2009 (Di Biagio, et al., 2010). The Onsala Space Observatory instrument (57° N, 12° E) measured CO in 2002–2008 (Forkman et al., 2012) and from 2014. The British Antarctic Survey (BAS) radiometer data set for Troll Station (72° S, 2.5° E) covers February 2008 to January 2010 (Straub et al., 2013). Each of these three ground-based instruments are microwave radiometers that measure emissions from molecules undergoing rotational transitions in the atmosphere, offering the advantage of providing measurements during polar night, compared to instruments that rely on the sun.

This paper presents a CO profile data set from 2008 to 2015 from measurements made by the Kiruna Microwave Radiometer (KIMRA) at the Swedish Institute for Space Physics, Kiruna (67.84° N, 20.41° E). KIMRA measurements during the winters 2008/09 and 2009/10 have previously been used (Hoffmann et al., 2011) to retrieve CO profiles that have been compared to satellite data from the Microwave Limb Sounder (MLS) aboard Aura, the Atmospheric Chemistry Experiment-Fourier Transform Spectrometer (ACE-FTS) aboard SCISAT-1, and the Michelson Interferometer for Passive Atmospheric Sounding (MIPAS) aboard Envisat. The comparisons showed good agreement below 60 km but at higher altitudes the profiles significantly diverged leading to a positive bias in KIMRA CO of

> 5 ppmv at 80 km. The shape of the bias in the profile was consistent between satellite data sets, and its origin is unclear.

This paper presents a CO data set from KIMRA, using an extended set of measurements, beginning in 2008 and retrieved using a new inversion setup. The structure of the paper is as follows: Sect. 2 provides details on the KIMRA observation system, i.e. the measurements and the inversion technique. Section 2 also offers an estimation of the errors in CO profiles and a word on the interpretation of the data. To establish validity of the observation system, Sect. 3 presents a comparison of the KIMRA data with MLS data, using temperature information from the Special Sensor Microwave Imager/Sounder (SSMIS) (Kunee et al., 2008; Swadely et al., 2008) aboard the US Air Force's Defense Meteorological Satellite Program F-18 satellite as input for the KIMRA CO inversion. Section 4 investigates changes in the retrieved KIMRA CO data when using temperature information from the European Centre for Medium-Range Weather Forecasting (ECMWF) and presents this extended data set, currently spanning 2008–2015. Section 5 concerns the availability and use of the data, and Sect. 6 offers some concluding remarks.

Satellite data are exchanged for ECMWF analysis in the KIMRA inversion in order to have a consistent temperature input for the entire KIMRA data set. The time span of continuing KIMRA measurements will generally surpass the lifetime of any satellite instrument. Many satellite instruments have well exceeded their mission lifetime, the three instruments mentioned in this section being good examples: MLS (2004–present), ACE-FTS (2003–present), and MIPAS (2002–2012). Ground-based instruments, however, have the potential to produce much longer data sets, albeit at one location, due to the much smaller cost of the ground-based projects and the ability to maintain the instruments. The Ozone Radiometer for Atmospheric Measurements, OZORAM, has been measuring ozone in the Arctic (79.9° N, 11.9° E) since 1994 (Palm et al., 2010), and Nedoluha et al. (2016) recently showed 20 years of chlorine monoxide measurements in the Antarctic (77.85° S, 166.77° E) with the Chlorine Oxide Experiment (ChLOE1). The Fourier transform infrared spectrometer at Kitt Peak (31.9° N, 111.6° W) (Brault, 1978) produces data sets beginning in the 1970s. These are just two examples of a large number of ground-based instruments. Long-term (decades) ground-based data sets are important as they reveal changes in the atmosphere on the timescale of changes in Earth's climate, and the data can be used to validate satellite instruments, fill gaps in time between satellite missions, and help combine satellite data sets that do not overlap in time.

2 Instrument and data set

2.1 KIMRA

KIMRA is housed at the Swedish Institute for Space Physics (IRF), Kiruna, and was partly designed by the In-

Table 1. More general details of KIMRA at a glance. Also see Sect. 2.1.

System noise temperature	~ 1800 K (single sideband)
Detector	Schottky diode at ~ 25 K
Sideband filter	Martin–Pupplett interferometer
Standing wave suppression	Path length modulator
Hot–cold calibration	Blackbodies at ~ 195 K/~ 293 K
Spectrometer	FFTS, bandwidth/resolution: 110 MHz/107 kHz

stitute for Meteorology and Climate Research (IMK) at the Karlsruhe Institute of Technology (KIT) (Raffalski et al., 2002). KIMRA utilises the frequency range of 195–233 GHz and has been measuring, among others, atmospheric spectra that correspond to the $J = 2 \rightarrow 1$ rotational transition (230.54 GHz) of CO. KIMRA has operated in Kiruna since 2002 and has been making measurements of CO emissions since 2008. The more general aspects of the instrument are given in Table 1, and more specific details can be found in Raffalski et al. (2002) and Hoffmann et al. (2011). The spectrometer used for CO measurements is a fast Fourier transform spectrometer (FFTS) made by Omnisys Instruments, with 1024 channels and used with a bandwidth of 110 MHz to give a resolution of ~ 107 kHz per channel. For a given measurement cycle, which includes multiple hot–cold calibrations and produces one time-averaged atmospheric spectrum, KIMRA points to the atmosphere at an elevation angle, between 5 and 90°, that is chosen to provide the best signal-to-noise ratio (SNR) at that time. This angle is governed by the atmospheric conditions and so can change from one measurement cycle to another. Because they are produced using different elevation angles, the individual spectra are not averaged to reduce the SNR. Spectral averaging has been used for similar measurements from other instruments that vary the elevation angle, e.g. over timescales of 1 week in Nedoluha et al. (2013) and 1 h in Ohyama et al. (2016). In the case of KIMRA, each spectrum is used to retrieve a CO profile, which may then be used in an average. The azimuth angle of a KIMRA measurement can change from one measurement cycle to another. The azimuth and elevation angle are kept constant during each measurement cycle. Figure 1a shows the distribution of the duration times of each measurement.

2.2 Inversion setup

CO profiles are retrieved from the spectra using an optimal estimation method (OEM) inversion (Rodgers, 2000). This is a Bayesian statistical approach that constrains the retrieved CO profile according to some a priori atmospheric information. The inversion was carried out using the Qpack 2 (Eriks-

son et al., 2005) package, which employs the Atmospheric Radiative Transfer Simulator (ARTS 2; Eriksson et al., 2011) to model radiative transfer through the atmosphere, i.e. the forward model. All of the following information that is input into the inversion is done so using Qpack 2. The a priori CO information used here is the average of one winter period (September through April) of output from the Whole Atmosphere Community Climate Model, version 4 (WACCM4) (Garcia et al., 2007) provided by Douglas Kinnison at the National Center for Atmospheric Research (NCAR), with a standard deviation of 100 % at all altitudes. This combination was found to give enough freedom to the inversion to fit expected changes in CO above Kiruna throughout a given winter period (here September through May) while providing enough regularisation of the retrieved solution so that no oscillations are readily observed in the CO profiles. The WACCM data are on a 132-layer grid between approximately the ground and 130 km. Ozone (O_3) is also retrieved simultaneously with CO, as there is an O_3 spectral line located at 231.28 GHz, and attenuation of the CO spectral line due to water vapour is accounted for by including the water vapour continuum described by Rosenkranz (1998) in the forward model and inversion. The spectroscopic information used is from the HITRAN (HIGH-resolution TRANsmission molecular absorption database) 2008 catalogue (Rothmann et al., 2009). Continua of molecular oxygen (O_2) and nitrogen (N_2) (Rosenkranz, 1993) and nitric acid (HNO_3) lines are also included in the inversion but are not retrieved and are considered model parameters. A priori profiles of O_3 , water vapour, and O_2 are from the same WACCM run as the CO a priori, and N_2 and HNO_3 a priori profiles are from the FASCOD (Fast Atmospheric Signature Code) subarctic winter scenario (Anderson et al., 1986). A priori profiles of CO, O_3 , water vapour, O_2 , and N_2 are unchanged from those described in Hoffman et al. (2011, 2012).

Measurement noise (statistical noise on the spectrum) was estimated by fitting a second-order polynomial to a wing of the spectrum and calculating the standard deviation of the fit. As there is no windowing applied in the operation of the FFTS, the spectrometer channels are specified in the inversion as having a sinc-squared response function (Harris, 1978). Three sine wave functions are fitted to the baseline of each spectrum during an inversion to account for errors in the baseline, which are most often produced by standing waves in the instrument. A fitting of functions to the baseline of the measurement (baseline fit) can be included in the optimal estimation performed by Qpack 2 and forms part of the general fit to the measurement (inversion fit). For sine waves, the period and estimated amplitude uncertainty are provided as input, and the amplitude and phase of the waves are retrieved. The periods of the sine waves in the KIMRA spectra were found by first inverting all of the measurements without a fit to the baseline and then evaluating a periodogram of the residuals. This procedure was also applied to subsets of the data in case some changes in the estimated periods

with time became evident. Sine waves in the baseline are not generally visible by eye on the CO spectra, but no changes over time were found in the determined wave periods. The periods of the fitted waves are 27.5, 55, and 36.3 MHz, with an estimated uncertainty in the amplitudes of 0.5, 0.3, and 0.5 K, respectively. These calculated sinewave periods are almost identical to those found by Hoffman et al. (2011) for the 2008/09 and 2009/10 winters (27.5, 55, and 36.6 MHz), and are similarly large in comparison to the width of the CO spectral line so that they are uniquely distinguishable from it. A second-order polynomial is also fitted to the baseline during the optimal estimation to account for any offsets or long-period sine wave signatures. The zeroth-, first-, and second-order coefficients have estimated uncertainties of 1, 0.5, and 0.5 K, respectively.

The altitude, pressure, and temperature information (zpT) for the inversion is constructed in two ways. For the first case, used in the comparison work with MLS (January 2011 to May 2014), information up to 10 hPa (~ 30 km) is from daily National Centres for Environmental Prediction (NCEP) profiles; information for 10–0.01 hPa (~ 30 –80 km: recommended range for use) is from SSMIS; and information above that is from the NRLMSISE-00 empirical model of the atmosphere (called MSIS hereafter) (Picone et al., 2002). Temperature data from SSMIS currently begin in January 2011 and end in June 2014. For the second case, used in the temporal extension of the KIMRA CO data set (2008–2015): the information up to 0.01 hPa is from ECMWF operational analyses output, and information above that is from MSIS. The SSMIS data set was used because it compares well with other satellite data sets (R. Larsson and P. Sheese, University of Toronto, personal communication, 2016) and has approximately four colocations (sets of measurements within 66–68° N, 15–25° E) with Kiruna per day. Around the altitudes at which the different temperature profiles are merged for use in the KIMRA inversion, the data are smoothed to avoid discontinuities in the final temperature profile. The inversions utilising SSMIS data are considered to be those using the most suitable available data for the CO inversion, as the sensitivity of KIMRA CO profiles to atmospheric temperature information is strongest within the retrievable altitude range (on average between 48 and 84 km), and the resulting CO data set is considered to be a reference point for inversion setups using alternate input temperature information.

The pressure grid used in the forward model is 250 layers, spaced approximately equally in altitude, between the ground and 125 km. The retrieval grid is a 62-layer subset of the forward model pressure grid with approximately 2 km spacing between the ground and 124 km. Using a subset of the forward model grid is recommended by Patrick Eriksson (first author of Qpack 2) as giving the most accurate mapping of information from the forward model grid to the retrieval grid during an inversion. A Marquardt–Levenberg iterative minimisation method (Marquardt, 1963) is used to perform a nonlinear inversion. The CO profile is retrieved in relative

units (as a fraction of the a priori) for numerical stability due to the strong gradients in atmospheric CO.

2.3 Characteristics of the retrieved data set

This section discusses the profiles retrieved using the NCEP–SSMIS–MSIS temperature information between 2011 and mid-2014. The inverted CO data set is restricted to the months of September–May, as summertime CO concentrations in the middle atmosphere are very low. The data are then further filtered to those that satisfy the following: a converged inversion, a degree of freedom for signal (DOFS) greater than 1 (DOFSs are calculated as the trace of the averaging kernel matrix; Rogers, 2000), a standard deviation of the fit residual no greater than 1.5 times the initial estimate of the measurement noise (to avoid overfitting the measurement), a mean of the fit residual that lies in the range (-1 , 1 K), and a baseline brightness temperature of < 230 K (an ad hoc indication of too cloudy weather). No filtering for outlying or anomalous concentration values was applied to the data. Overall, 28 % of the data was identified as unusable, with the DOFS criteria being responsible for about half of that number. If one finds this a high rejection rate, bear in mind that KIMRA operates regardless of weather conditions, and CO concentrations may be very low in time periods near the beginning and end of winter. The fact that measurements during very low middle-atmospheric CO concentrations are more likely to be filtered out means that the KIMRA CO data set may have an average CO value that is higher than the true atmosphere value.

Figure 1b shows an example spectrum of a CO measurement with KIMRA and the corresponding inversion fit. The inversion fit includes the baseline fit described in Sect. 2.2 and the example baseline fit is plotted alongside the residual in Fig. 1 for comparison. Considering the entire data set, the standard deviation (averaged across all spectrometer channels) of the amplitude of the fitted baseline is 0.21 K, and the average standard deviation of the residual is 0.34 K. In other words, changes in the retrieved amplitude of the baseline are, on average, lower than the statistical measurement noise on the spectrum.

The mean of the averaging kernels for the CO data set is also shown in Fig. 1c along with the measurement response (Fig. 1d) (sum of the rows of the averaging kernel matrix) and the altitude resolution of the profiles (full width at half maximum (FWHM) of the averaging kernels). Altitudes with a measurement response greater than 0.8 are considered to represent the range of useful profile information: the retrievable altitude range. This choice is somewhat arbitrary, with 0.8 being a regularly used value (e.g. Forkman et al., 2012; Hoffmann et al., 2011; Straub et al., 2013). The CO profiles here have an average retrievable altitude range of 48–84 km and an average vertical resolution of between 15 and 18.5 km depending on the altitude. These compare to an average altitude range of 40–80 km and average resolution of 16–22 km for

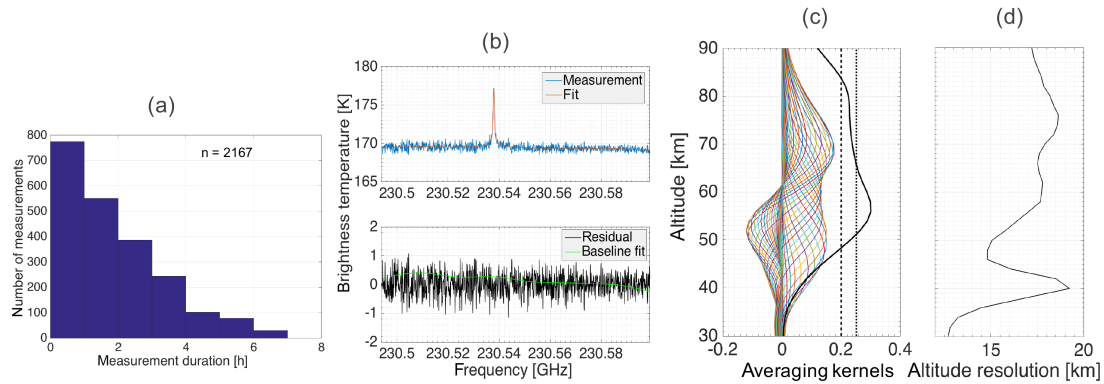


Figure 1. (a) A histogram of the KIMRA CO measurement durations from January 2011 to May 2014 with n as the number of measurements (see Sect. 2.2). (b) Upper: an example measurement from 5 November 2012 with the corresponding inversion fit (which includes the baseline fit; see Sect. 2.2). Lower: the residual (measurement minus inversion fit) and the baseline fit for comparison. (c) The mean averaging kernels for all CO measurements, with the measurement response divided by 4 shown in black. The dashed and dotted black lines indicate a measurement response of 0.8 and 1.0, respectively. (d) The corresponding mean altitude resolution of the CO profiles, derived from the FWHM of the averaging kernels.

the CO profiles shown in Hoffmann et al. (2011) for the winters of 2008/09 and 2009/10. DOFSs for the current data set have a mean of 2.0 and a standard deviation of 0.6. The minimum and maximum of the lower and upper retrieval limit for the current data set is 35 and 99 km, respectively, but the upper limit of any profile (defined using measurement response) must be considered with the following caveat.

The centres of the averaging kernels, when represented in VMR, are shifted down in altitude compared to a representation using relative concentrations. Hoffmann et al. (2011) provide a detailed discussion of the representation of averaging kernels for ground-based CO measurements, and the major points are worth repeating here. While here the lower limits of the retrievable altitude ranges are set by the SNR of the measurement, the upper limit of the measurements is set by the transition from a pressure-broadening regime to a Doppler-broadening regime (not considering spectrometer channel resolution). The result of this is that, above approximately 70 km in the VMR representation, the altitude locations of the centres of the averaging kernels do not increase anymore with the increase in respective retrieval altitude. And while the retrieved CO values above 70 km do contain information from the atmosphere corresponding to the retrieval altitude, the VMR representation of the data above this altitude should be considered with care.

2.4 Error estimates for the retrieved data set

Errors in the retrieved CO profiles arise from uncertainties in instrumental parameters and in parameters that are used as input to the forward model. The relative contributions from these uncertainties are calculated here using the OEM error definitions and by introducing perturbations to the inputs. OEM error definitions are described in detail in Rodgers (2000), among others, and are not repeated here. Figure 2

shows the estimated contributions to the CO profile error budget from the following uncertainties. There are, of course, possible sources of error in any stage of the instrumentation, and the parameters discussed here are considered to represent the dominant uncertainties.

The statistical noise, ΔT , on a spectrum is governed by the so-called radiometer equation $\Delta T = T_{\text{sys}}/\sqrt{\nu\tau}$, with T_{sys} as the system noise temperature of the instrument, $\Delta\nu$ as the channel bandwidth (Table 1), and τ as the integration time for a measurement of the atmospheric signal. The uncertainty for the temperature profile used in an inversion is the same uncertainty used in Hoffman et al. (2011): 5 % below 80 km, 10 % above 100 km, and linearly interpolated in between. Uncertainties in the spectroscopic parameters of the CO line are from the HITRAN 2008 catalogue and are 1 % for the line intensity, 2 % for the air broadening parameter, and 5 % for the temperature dependence of air broadening. Uncertainty in the line position is ignored as the frequency grid can be adjusted to match the line centre in a measurement, and the parameters associated with self-broadening are considered as having negligible impact due to the relatively low concentration of the observed gas (Ryan and Walker, 2015). For the blackbody targets used in the calibration of the atmospheric measurement, an uncertainty of 2 K is assumed in the temperature of the hot and cold target: a conservative estimate that accounts for fluctuations and drifts in temperature. The uncertainty in the pointing of the instrument to the sky is estimated as 1° . This is 1 order of magnitude higher than the precision of the motor that controls pointing, to allow for a possible offset in the orientation of KIMRA.

The resulting error estimates as well as a sum, in quadrature, of the errors are plotted in Fig. 2 and show that the predominant error in the CO profiles comes from the statistical measurement noise on the spectrum. This peaks at 30 %

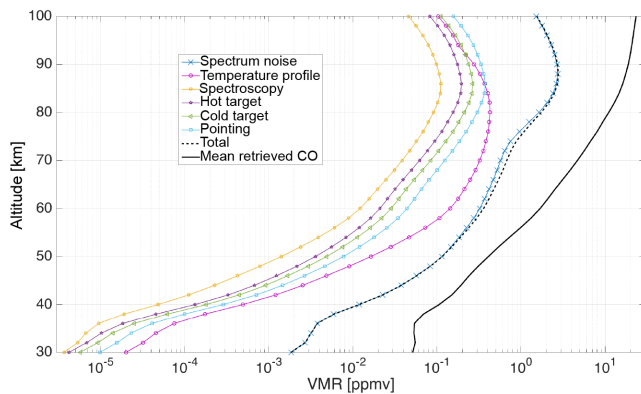


Figure 2. Estimated profiles of error for the KIMRA CO profiles. Section 2.4 describes the sources of uncertainties used to estimate the errors. The error due to spectrum noise is an average value over all measurements, and the other errors are calculated about the KIMRA CO a priori profile.

of the mean KIMRA CO profile, at 53 km altitude. The error from uncertainties in the temperature profile also shows a significant contribution to the total error in the retrievable altitude range above approximately 60 km. The error due to noise on the spectrum is calculated during each inversion and is provided in the supplemental data with the corresponding CO profiles. The error profile in Fig. 2 is an average over all measurements. The other plotted errors are calculated about the a priori CO profile and serve as an estimate of the respective error contributions to each measurement. To calculate these errors for individual measurements is computationally expensive, and so the values plotted in Fig. 2 are provided with the available KIMRA CO data (see Sect. 5).

2.5 Smoothing error and interpretation of the KIMRA profiles

The smoothing error in the profiles arises from the limited vertical resolution of the retrieved profile and can be calculated with the OEM using the averaging kernels and a priori information for a profile. The smoothing error can be large for ground-based profiling instruments due the small altitude spacing between retrieval grid points, chosen here for numerical stability in the inversion (Eriksson, 1999), compared to the actual vertical resolution of the retrieved profiles (see Fig. 1c and d). Smoothing error should be assessed when one wishes to use or interpret the CO profiles without consideration of the accompanying averaging kernels. As this is not a recommended use of the data, the smoothing error is not assessed here. If using KIMRA profiles to say something of the absolute value of CO at a given retrieval altitude, one must be aware that a CO value at a retrieval grid point contains information from a range of altitudes with a sensitivity governed by the shape of the corresponding averaging kernel.

The smoothing error can be accounted for when comparing KIMRA CO profiles to those of an instrument/model that has a significantly different vertical resolution by using the KIMRA averaging kernel matrices and a priori to smooth (Rodgers and Connor, 2013) the other profiles so that they have a similar vertical resolution. KIMRA profiles can be used to observe changes in CO concentrations over time, provided there is no significant difference in the averaging kernels (and thus measurement response) of the profiles over that time. In particular, care should be taken with data near the edges of the retrievable altitude range (where the measurement response is decreasing towards 0.8), as the measurement response in this region can change quickly when there are sharp changes in atmospheric CO.

3 Comparison with MLS

This section presents a comparison of CO profiles from KIMRA and MLS that are colocated in space and time. A description of the MLS instrument is given in Waters et al. (2006). Version 4.2 of the CO data (Schwartz et al., 2015) is used here, a description of which can be found in Livesey et al. (2015). Version 4.2 CO data cover the pressure range of 215–0.0046 hPa. The precision of the CO profile reaches a maximum (largest) value of 1.1 ppmv at the highest retrieval layer (0.0046 hPa). In the middle atmosphere the data set has a positive bias of approximately 20 % compared with the ACE-FTS satellite instrument. This estimate is given by Livesey et al. (2015) using a validation of the MLS version 2.2 CO data (Pumphrey et al., 2007), which showed a positive bias of approximately 30 %: later versions than 2.2 show a slight lowering of the MLS values, bringing them closer to the ACE-FTS data.

3.1 Colocation of KIMRA and MLS measurements

For a given KIMRA measurement, a coincident MLS measurement was defined as follows. MLS measurements that were made within 4 h, $\pm 2^\circ$ latitude, and $\pm 10^\circ$ longitude of the KIMRA measurement and lie in the same position relative to the vortex edge as the KIMRA measurement (inside, outside, or within the edge of the polar vortex) were identified. The MLS measurement from this group that was closest, along a great circle, to the KIMRA measurement was chosen as coincident. A given KIMRA–MLS measurement could only be considered coincident with one MLS–KIMRA measurement. The location of a measurement with respect to the polar vortex was determined using scaled potential vorticity (sPV) values from NASA’s Global Modeling and Assimilation Office’s (GMAO’s) MERRA (Modern Era Retrospective analysis for Research and Applications) (Rienecker et al., 2011). The sPV values for KIMRA were calculated geometrically along the instrument’s line of sight. sPV values of 1.6 and $1.2 \times 10^{-4} \text{ s}^{-1}$ have been used extensively in previous works (e.g. Manney et al., 1994, 2007, 2011; Jin et

al., 2006) to define the respective inner and outer edge of the vortex, and the same values are used here.

The location of a measurement, its position relative to the vortex, and the distance between measurements were calculated at 50 km altitude. The position relative to the vortex changes with altitude, which means that a single profile may simultaneously contain information from inside, outside, and the edge of the polar vortex. The altitude chosen to define the three positions relative to the vortex is 50 km because it divides the CO measurements from KIMRA into the three most distinct populations of concentration values. This was tested by using different altitudes to define the position relative to the vortex, calculating partial (46–66 and 66–86 km) CO column concentrations and testing whether the column concentrations were significantly different from each other when grouped by vortex relative position. This is not to say that there should always be three distinct air masses of CO, but it can be expected based on the strong cross-vortex gradient of the gas (see Sect. 1). The strong CO gradient during winter has recently been used in a chemical definition of the mesospheric vortex (Harvey et al., 2015).

Figure 3 shows the results for the KIMRA CO columns with vortex relative positions calculated using sPV values at 40, 50, and 60 km. The sPV information is available up to approximately 62 km. Using 40 km, the partial columns defined as outside and in the edge of the vortex are statistically indistinguishable at the 5% significance level using an unpaired two-sample *t* test, and using 60 km, the inside and edge of vortex 46–66 km partial columns are indistinguishable. With the same test and using 50 km, the three groups of partial columns comprise three distinct populations of concentration values in both the stratosphere and the mesosphere. Using other altitudes to define the vortex relative position also produced distinguishable concentrations, and 50 km was chosen as it gives the most distinct vortex relative concentration values in both the stratosphere and mesosphere and also because the sPV-defined location of the vortex edge in the upper stratosphere becomes much less well-defined as the winter progresses (Manney et al., 1997). Both the sPV and CO concentration gradients will be less distinct before/after and during the formation/breakdown of the polar vortex.

3.2 Comparison of colocated measurements

There are 916 coincident profiles found using the criteria in the previous section. The MLS CO profiles have a vertical resolution more than twice as fine as that of the KIMRA profiles: 3.5–5 km from the upper troposphere to the lower mesosphere and 6–7 km in the upper mesosphere (Livesey et al., 2015). Because of this, the MLS profiles were smoothed with the averaging kernels of coincident KIMRA profiles to account for the difference in vertical resolution. MLS CO profiles are retrieved up to 0.001 hPa in the atmosphere and use a constant CO concentration above this. Because there is some low sensitivity of the KIMRA CO profiles to atmo-

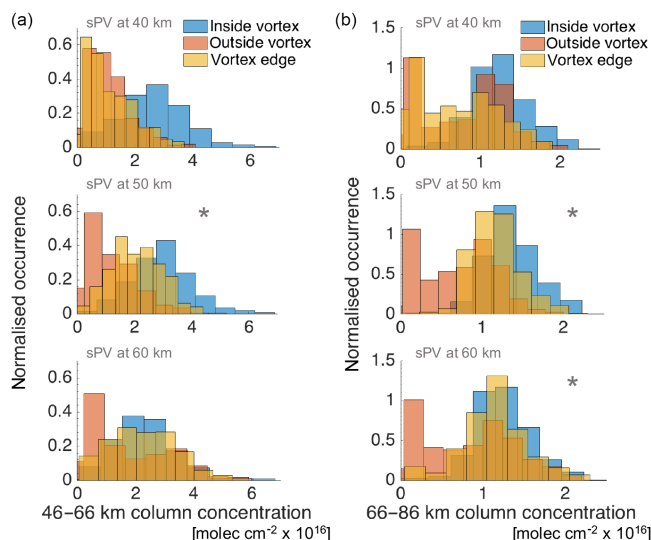


Figure 3. The distributions of KIMRA CO partial (46–66 and 66–86 km) column concentrations divided into groups defined by their position relative to the polar vortex edge using sPV (see Sect. 3.1). The relative positions are calculated using sPV values at 40, 50, and 60 km, as indicated on respective plots. Using sPV at 50 km gives the three most distinct distributions, as calculated with an unpaired two-sample *t* test (see Sect. 3.1). The asterisks indicate plots with three distinct distributions.

spheric concentrations above this (see the averaging kernels in Fig. 1), the MLS profiles were extrapolated from 0.001 hPa before smoothing. A linear extrapolation in pressure space was used to extend the MLS profiles instead of using scaled KIMRA a priori information so as to avoid creating artificial agreement between KIMRA and MLS. Figure 4 shows the mean of the extrapolated and the original MLS profiles, as well as the KIMRA a priori for comparison. The extrapolated profile is considered a more realistic representation of the atmosphere than the constant value provided for MLS at these altitudes. MLS values at 82 and 84 km are often defined as unusable for scientific work due to an a priori contribution that is too high (Livesey et al., 2015), and the precision is given as negative in this case. The CO values are still considered here as useful for comparative purposes, but quantities derived using the precision (e.g. the slope of a line) are not meaningful at these altitudes. Figure 5a–e show the results of the comparison of the 916 pairs of coincident CO profiles found between January 2011 and May 2014. The means of KIMRA and MLS CO profiles are shown (Fig. 5a) as well as the mean of the differences (bias) in the coincident profiles in ppmv (Fig. 5b) and relative to the mean of KIMRA and MLS profiles (Fig. 5c), the sample Pearson correlation coefficient for the profiles at each altitude (Fig. 5d), and the slope of a line of best fit to KIMRA vs. MLS at each altitude layer (Fig. 5e), explained below. The times between coincident measurements and the location of the coincident MLS profiles are also shown (Fig. 5f). The statistics in Fig. 5 are

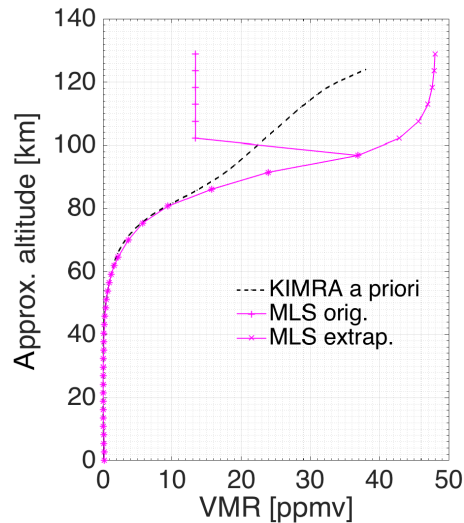


Figure 4. The mean of the coincident MLS CO profiles and the a priori CO profile used for the KIMRA inversion (Sect. 2.2). “MLS orig.” shows the mean of the supplied MLS profiles, which use a constant CO concentration above 0.001 hPa (~ 98 km). “MLS extrap.” shows the mean of the profiles that have been linearly extrapolated in pressure space above 0.001 hPa to provide more physical CO concentrations at these altitudes.

calculated using all colocated pairs of profiles and are also assumed to be representative of subsets of the data as there appears to be no particular time of the year during which the differences are more/less pronounced.

The mean profiles show a maximum absolute bias of ~ 0.65 ppmv at 68 km and a maximum relative bias of 22 % (0.44 ppmv) at 60 km, with bias being defined as KIMRA minus MLS. The standard deviation of the differences in the profiles peaks at 21 % at 60 km. These standard deviation values are similar in magnitude to the estimated uncertainties in the KIMRA CO profiles (Fig. 2). The standard error on the bias is not shown in Fig. 5b and c because it is very small due to the number of coincidences, but rather the standard deviation of the differences is shown as the whiskers on the bias. The combination defines a 1σ space in which a KIMRA profile lies with respect to an MLS profile. The correlation of the profiles is high at all altitudes, only dropping below 0.90 above 82 km. The correlation between KIMRA and unsmoothed MLS profiles is also plotted, with values between 0.81 and 0.90. Previous CO retrievals for winter 2008/09 and 2009/10 (Hoffmann et al., 2011) showed a bias with respect to MLS, increasing with altitude, with a value of > 5 ppm at 80 km. The structure of this bias was also shown in comparisons of KIMRA with ACE-FTS and MIPAS, and it appears that this attribute is not present in the retrievals presented here.

The slope of a line of best fit to KIMRA vs. MLS measurements was calculated individually for each altitude layer as follows: for a given retrieval grid point the slope and in-

tercept (or regression coefficients) for a line of best fit to the KIMRA and MLS values was calculated, accounting for errors in the abscissa (MLS) and ordinate (KIMRA) values according to York et al. (2004). Two cases of KIMRA CO error estimates were used when calculating a line of best fit: the first being the measurement error in the profile (the error due to statistical noise on the spectrum; Sect. 2.4) and the second being twice the measurement error. The former is an underestimation of the true error on the profile as there are more error sources than measurement error alone, and the latter is likely an overestimation of the true error as the measurement error is a predominant source of error in the profile (Fig. 2). The results (Fig. 5e) show that the slope is always greater than the ideal value of 1.0 for both KIMRA error estimates, meaning that KIMRA shows a greater range of CO concentrations at all altitudes and the variation is not explained by the estimated random errors in the profile. The reason for the difference could be due to errors, e.g. spectroscopic information, calibration, and baseline wave signatures, that can have a contribution that is neither truly systematic nor random. The difference in calculated slopes for the two KIMRA error estimates is insignificant within the standard error, likely due to the large natural variation in CO concentrations. Despite the > 1.0 slope values, KIMRA and MLS are considered to show agreement, according to the level of difference and correlation between profiles.

4 Extension of the KIMRA data set

After establishing a reliable inversion scheme through comparison with MLS, the KIMRA data set is extended in time by substituting ECMWF operational analyses model output for the SSMIS temperature data in the inversion (see Sect. 2.2).

4.1 The effect of temperature input on KIMRA CO profiles

ECMWF temperatures are available four times per day, in 6-hourly intervals beginning at midnight. The same filtering procedure for the retrieved data is employed as outlined in Sect. 2.3. To evaluate the effect of using a different temperature data set as input to the inversion, the two KIMRA data sets are compared where they overlap between January 2011 and May 2014, and the results are shown in Figs. 6 and 7.

A comparison of the two sets of temperature profiles (ECMWF–MSIS minus/vs. NCEP–SSMIS–MSIS) is shown in Fig. 6. Figure 6a and b show the mean and standard deviation of the differences between temperature profiles in absolute and relative units, Fig. 6c shows the correlation at each altitude, and Fig. 6d shows the slope of the lines of best fit at each altitude. The same is shown for the two respective sets of CO profiles in Fig. 7. No smoothing with averaging kernels is applied to the data.

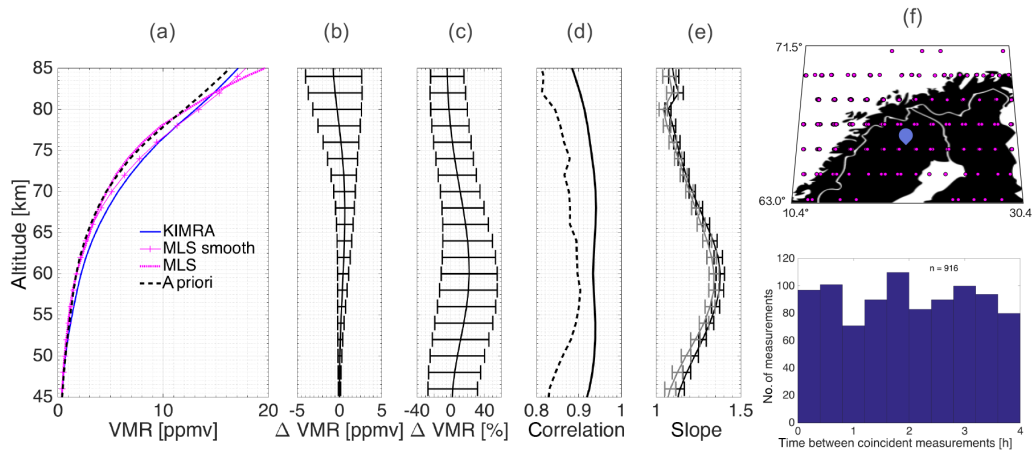


Figure 5. (a) The means of the coincident KIMRA and MLS CO profiles from 2011 to 2014, the mean of the unsmoothed MLS profiles, and the a priori profile used for the KIMRA inversion. (b) The mean of the difference between the KIMRA and smoothed MLS profiles with the standard deviation of the differences as the whiskers on the line. (c) The same as (b) but in relative units, as percent of the mean of KIMRA and MLS CO profiles. (d) The correlation coefficients of KIMRA and smoothed (solid) and unsmoothed (dashed) MLS data. (e) The slope and standard error of a line of best fit to KIMRA vs. smoothed MLS, calculated at each level using given MLS error estimates and two estimations of KIMRA error: the measurement error (black) and double the measurement error (grey) (see Sect. 3.2). The slope values at 82 and 84 km are unreliable as MLS precision is often quoted as negative at these altitudes. (f) The location of the MLS measurements (magenta) with respect to Kiruna (blue) and a histogram of the times between coincident measurements. n is the number of pairs of colocated profiles. The temperature input for the KIMRA inversions shown here includes SSMIS data (see Sect. 2.2).

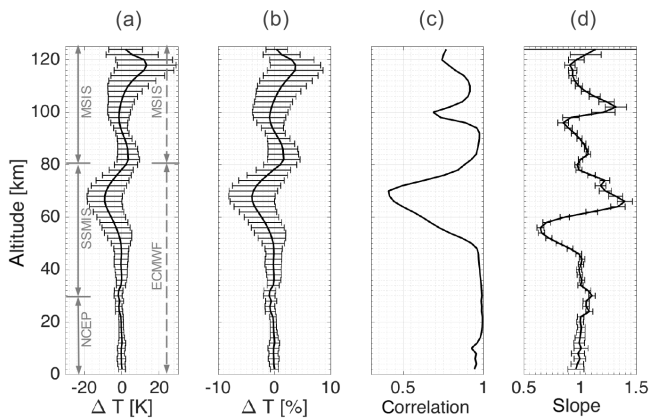


Figure 6. (a) The absolute mean of the difference in the temperature profiles (ECMWF–MSIS minus NCEP–SSMIS–MSIS) used in the two inversion setups for KIMRA. The altitude ranges of the temperature information used in the profiles (see Sect. 2.2) are shown here. (b) The mean of the percentage difference in the profiles (difference divided by the average of the two profiles). (c) The correlation between the two data sets. (d) The slope of a line of best fit to the data sets at each level, with ECMWF–MSIS as the dependant (Y) variable. The slope value at the highest altitude shown has a relatively large standard error because of the lower number of points at this altitude after conversion from a pressure to an altitude grid.

The bias for the temperature profiles is very low below 50 km, showing good agreement between ECMWF and NCEP output, as well as the lower-altitude SSMIS data, and then moves to a minimum of $\sim -4\%$ at 68 km. The max-

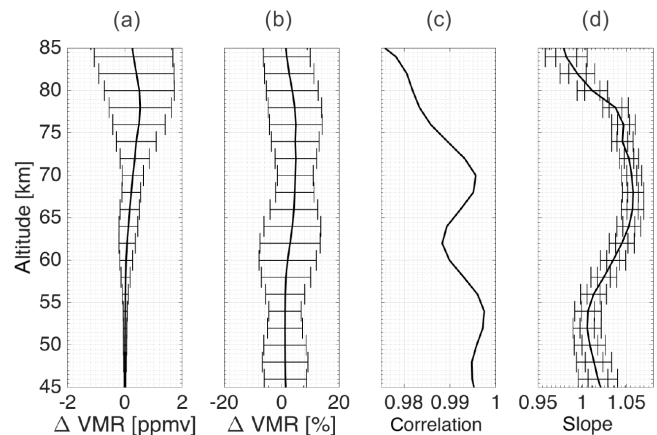


Figure 7. (a–d) The same calculations as shown in Fig. 6 but for the CO volume mixing ratios retrieved using the respective temperature data sets. The slopes and their standard errors (d) are calculated with the same two KIMRA error estimates as in Fig. 4 (see Sect. 3.2), with the larger error bars corresponding to the larger error estimate. Note the different altitude range compared to Fig. 6.

imum in the bias is about 4% at 118 km. The correlation is high below 50 km but has minima of < 0.50 at ~ 70 km and ~ 0.80 at 100 km. It should be noted that while MSIS is used in both temperature data sets, the time of the MSIS output is governed by the times for the ECMWF output and the SSMIS measurements, and so the high-altitude (> 0.01 hPa) temperature values are not necessarily equal for the two inversion setups. The slopes of the lines of best fit were calcu-

lated using the same temperature error estimate, as described in Sect. 2.4, for each data set. The slope is within 11 % of 1.0 below 50 km altitude, above which it decreases to around 0.65 at 56 km before increasing to 1.4 at 66 km and then varies about 1 with another peak of 1.3 at 102 km.

There is a general positive bias in the CO profiles that use ECMWF–MSIS, seen in Fig. 7a and b. The bias is small, reaching a maximum of $\sim 5\%$ in the range of 68–78 km. The correlation of the profiles is very high, greater than 0.98 at all altitudes below 82.5 km. The slopes of the lines of best fit were calculated with the same error estimates described in Sect. 3.2. A value of 1.0 lies in the range of standard error of the slope below 56 km and above 80 km and between these altitudes reaches a maximum of 1.06. As the only difference in the inversion setups is the temperature input, it follows that any inequalities of the respective KIMRA CO profiles are ultimately due to this difference. Overall, the CO profiles using the differing temperature inputs shown here agree very well.

4.2 KIMRA CO data set from 2008 to 2015

Figure 8 shows the KIMRA CO data set between December 2008 and May 2015. Daily averaged CO concentrations between 46 and 86 km are shown. Data gaps in this time range are due to non-operation of the instrument or a lack of CO spectral line measurements. Data from winter 2015/16 are unavailable due to a failure of the KIMRA cooling system.

While it is impossible to fully characterise the concentrations shown without inclusion of other instrument data and/or model output, some observations are made here. The beginning of each winter (from about September through November) shows a movement of CO to lower altitudes, which can in general be expected as predominantly due to vertical advection (Allen et al., 1999; Minschwaner et al., 2010; Solomon et al., 1985). The high CO concentrations remain for most of winter before decreasing again from March onwards, generally due to loss of CO because of increased $\cdot\text{OH}$ and movement of low-CO air from lower latitudes as the final warming of the pole occurs. Signatures of “major” SSWs (during which the 10 hPa zonal circulation becomes easterly at 60°N), beginning 24 January, 26 January, and 6 January, 2009, 2010, and 2013, respectively, can be seen by the quickly (order of days) decreasing CO concentrations around these dates and then the subsequent increases as the vortex recovered (see Sect. 1) (Manney et al., 2009, 2015). The effects of a “minor” SSW (during which the 10 hPa zonal circulation remains westerly at 60°N) in early January 2015 (Manney et al., 2015) can also be seen. Decreases in CO concentrations during SSWs are mainly due to the influx of lower-latitude air as the polar vortex destabilises. There are other visible fluctuations in the presented KIMRA CO data over various timescales which, while not interpreted here, can be used in the characterisation of winter-time dynamics above Kiruna.

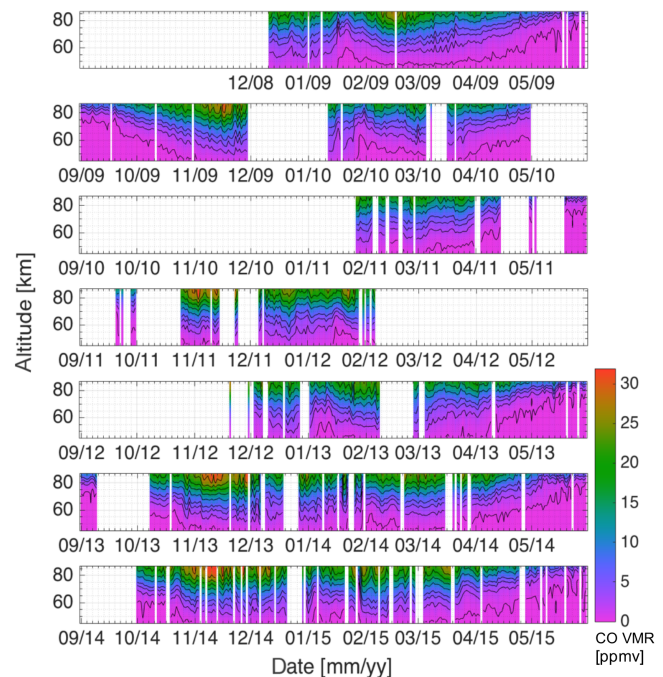


Figure 8. Daily averaged CO volume mixing ratios (in ppmv) above Kiruna from December 2008 through May 2015. Blank areas within this time are gaps in the data record. Data are plotted using the Isoluminant colour map from Kindlmann et al. (2002), and non-uniformly spaced contours (black lines) between 0.4 and 28 ppmv are added to guide the eye. The temperature input for the KIMRA inversions shown here includes ECMWF analysis (see Sect. 2.2).

5 Data availability

The current KIMRA CO data set (between December 2008 and May 2015) can be accessed publically through PANGAEA Data Publisher for Earth and Environmental Science at doi:10.1594/PANGAEA.861730. Metadata are also provided, including the averaging kernel matrices for each measurement. It is recommended to use the averaging kernels specific to each CO profile when using the data in a comparison with model output or a data set with significantly different altitude resolution.

6 Conclusion

The aim of this work was to create a self-consistent data set of strato-mesospheric CO profiles above Kiruna, using measurements from the ground-based microwave radiometer, KIMRA, and an optimal estimation technique. The resulting profiles cover an average altitude range of 48–84 km. The retrievable altitude limits vary with the SNR of each measurement, and CO VMRs above 70 km should be treated with care due an offset in centres of the corresponding averaging kernels above this altitude. As a test of the validity of the KIMRA observing system and to create a reference data

set, CO was first retrieved using atmospheric temperature information from the SSMIS satellite instrument, available in 2011–2014 and compared to CO data from MLS. The instruments show agreement, with KIMRA showing a maximum bias of ~ 0.65 ppmv at 68 km (corresponding to 14.7 % of the mean CO value at 68 km) and a maximum relative bias of 22 % (0.44 ppmv) at 60 km. Correlations with MLS are greater than 0.90 at most altitudes. KIMRA shows a larger range of atmospheric CO concentrations, compared to MLS, that is not explained by the estimates of random errors in the data and may be due to some combination of random and systematic uncertainty. Some differences in the KIMRA and MLS data can be expected due to imperfect collocation of the measurements and because MLS has a horizontal resolution of 200–300 km in the mesosphere and stratosphere: 1 order of magnitude wider than the beamwidth of KIMRA at these altitudes. The KIMRA data set is extended in time (2008–2015) by substituting ECMWF operational analyses temperature output in place of the SSMIS data. The extended KIMRA data set shows a difference (bias) of less than 5 % compared to the reference data set (the one using SSMIS data), and correlations between the two are greater than 0.98 at most altitudes. There is a larger range (≤ 6 %) of concentrations seen by the extended data set, compared to the reference data set over the same time period. The extended data set currently spans the time between December 2008 and May 2015, with data gaps. Measurements are ongoing at IRF Kiruna.

Author contributions. Mathias Palm designed and took an active role in the project. Niall J. Ryan developed the inversion setups for KIMRA and performed the comparisons. Richard Larsson provided SSMIS temperature data. Gloria Manney and Luis Millán provided sPV information for KIMRA measurements. Uwe Raffalski maintains KIMRA and provided the KIMRA measurement data. Justus Notholt provided valuable feedback on the project. Niall J. Ryan prepared the paper with contributions from coauthors.

Competing interests. The authors declare that they have no conflict of interest.

Acknowledgements. This work has been funded by the German Federal Ministry of Education and Research (BMBF) through the research project: Role Of the Middle atmosphere in Climate (ROMIC), sub-project ROMICCO, project number 01LG1214A. We would like to express our gratitude to the MLS teams for making their CO and sPV products available. We would also like to thank the ECMWF and NCEP teams for making their products available, as well as the Qpack and ARTS communities for making their software available. Work at the Jet Propulsion Laboratory, California Institute of Technology, was done under contract with the National Aeronautics and Space Administration. We thank the editor and three anonymous referees for their valuable input to the

paper. Thank you to Dagmar Eikenroth, Gerrit Armbrecht, and Helen Imhoff for making the published version of the paper look nice.

The article processing charges for this open-access publication were covered by the University of Bremen.

Edited by: D. Carlson

Reviewed by: three anonymous referees

References

- Allen, D. R., Stanford, J. L., López-Valverde, M. A., Nakamura, N., Lary, D. J., Douglass, A. R., Cerniglia, M. C., Remedios, J. J., and Taylor F. W.: Observations of Middle Atmosphere CO from the UARS ISAMS during the Early Northern Winter 1991/92, *J. Atmos. Sci.*, 56, 563–583, 1999.
- Anderson, G. P., Clough, S. A., Kneizys, F. X., Chetwynd, J. H., and Shettle, E. P.: AFGL atmospheric constituent profiles (0–120 km), Air Force Geophysics Laboratory, HANSCOM AFB, MA, USA, Environmental Research Papers, No. 954, AFGL-TR-86-0110, 1986.
- Brault, J. W.: Solar Fourier transform spectroscopy, in: Proceedings of the JOSO workshop, future solar optical observations, needs and constraints, November 1978, Firenze, Italy, 32–52, 1978.
- Damiani, A., Funke, B., Puertas, M. L., Gardini, A., Santee, M. L., Froidevaux, L., and Cordero, R. R.: Changes in the composition of the northern polar upper stratosphere in February 2009 after a sudden stratospheric warming, *J. Geophys. Res.-Atmos.*, 119, 11429–11444, doi:10.1002/2014JD021698, 2014
- Di Biagio, C., Muscari, G., di Sarra, A., de Zafra, R. L., Eriksen, P., Fiocco, G., Fiorucci, I., and Fuà, D.: Evolution of temperature, O₃, CO, and N₂O profiles during the exceptional 2009 Arctic major stratospheric warming observed by lidar and mm-wave spectroscopy at Thule (76.5° N, 68.8° W), Greenland, *J. Geophys. Res.*, 115, D24315, doi:10.1029/2010JD014070, 2010.
- Eriksson, P.: Microwave radiometric observations of the middle atmosphere: simulations and inversions, PhD thesis, Chalmers University of Technology, Göteborg, Sweden, 1999.
- Eriksson, P., Jimenez, C., and Buehler, S. A.: Qpack, a general tool for instrument simulation and retrieval work, *J. Quant. Spectrosc. Ra.*, 91, 47–64, 2005.
- Eriksson, P., Buehler, S. A., Davis, C. P., Emde, C., and Lemke, O.: ARTS, the atmospheric radiative transfer simulator, Version 2, *J. Quant. Spectrosc. Ra.*, 112, 1551–1558, 2011.
- Forkman, P., Christensen, O. M., Eriksson, P., Urban, J., and Funke, B.: Six years of mesospheric CO estimated from ground-based frequency-switched microwave radiometry at 57° N compared with satellite instruments, *Atmos. Meas. Tech.*, 5, 2827–2841, doi:10.5194/amt-5-2827-2012, 2012.
- Garcia, R. R., Marsh, D. R., Kinnison, D. E., Boville, B. A., and Sassi, F.: Simulation of secular trends in the middle atmosphere, 1950–2003, *J. Geophys. Res.*, 112, D09301, doi:10.1029/2006JD007485, 2007.
- Harris, F. J.: On the Use of Windows for Harmonic Analysis with the Discreet Fourier Transform, *Proceedings of the IEEE*, 66, 51–83, 1978.

- Harvey, V. L., Randall, C. E., and Collins, R. L.: Chemical definition of the mesospheric polar vortex, *J. Geophys. Res.-Atmos.*, 120, 10166–10179, doi:10.1002/2015JD023488, 2015.
- Hoffmann, C. G., Raffalski, U., Palm, M., Funke, B., Golchert, S. H. W., Hochschild, G., and Notholt, J.: Observation of strato-mesospheric CO above Kiruna with ground-based microwave radiometry – retrieval and satellite comparison, *Atmos. Meas. Tech.*, 4, 2389–2408, doi:10.5194/amt-4-2389-2011, 2011.
- Hoffmann, C. G., Kinnison, D. E., Garcia, R. R., Palm, M., Notholt, J., Raffalski, U., and Hochschild, G.: CO at 40–80 km above Kiruna observed by the ground-based microwave radiometer KIMRA and simulated by the Whole Atmosphere Community Climate Model, *Atmos. Chem. Phys.*, 12, 3261–3271, doi:10.5194/acp-12-3261-2012, 2012.
- Jin, J. J., Semeniuk, K., Manney, G. L., Jonsson, A. I., Beagle, S. R., McConnell, J. C., Dufour, G., Nassar, R., Boone, C. D., Walker, K. A., Bernath, P. F., and Rinsland, C. P.: Severe Arctic ozone loss in the winter 2004/2005: observations from ACE-FTS, *Geophys. Res. Lett.*, 33, L15801, doi:10.1029/2006GL026752, 2006.
- Kindlmann, G., Reinhard, E., and Creem, S.: Face-based lightness Matching for Perceptual Colormap Generation, *IEEE Proceedings of the conference on Visualization 2002*, available at: www.cs.utah.edu/~gk/papers/vis02/FaceLumin.pdf, 2002.
- Kunkee, D. B., Poe, G. A., Boucher, D. J., Swadely, S. D., Hong, Y., Wessel, J. E., and Uliana, E. A.: Design and Evaluation of the First Special Microwave Imager/Sounder, *IEEE T. Geosci. Remote.*, 46, 863–883, 2008.
- Lee, J. N., Wu, D. L., Manney, G. L., Schwartz, M. J., Lambert, A., Livesey, N. J., Minschwaner, K. R., Pumphrey, H. C., and Read, W. G.: Aura Microwave Limb Sounder observations of the polar middle atmosphere: Dynamics and transport of CO and H₂O, *J. Geophys. Res.*, 116, D05110, doi:10.1029/2010JD014608, 2011.
- Livesey, N. J., Read, W. G., Wagner, P. A., Froidevaux, L., Lambert, A., Manney, G. L., Millán Valle, L. F., Pumphrey, H. C., Santee, M. L., Schwartz, M. J., Wang, S., Fuller, R. A., Jarnot, R. F., Knosp, B. W., and Martinez, E.: Version 4.2x Level 2 data quality and description document, Jet Propulsion Laboratory, California Institute of Technology Pasadena, California, USA, Tech. rep., JPL D-33509 Rev. A, 162 pp., 2015.
- Manney, G. L., Zurek, R. W., O'Neill, A., Swinbank, R., Kumer, J. B., Mergenthaer, J. L., and Roche, A. E.: Stratospheric warmings during February and March 1993, *Geophys. Res. Lett.*, 21, 813–816, 1994.
- Manney, G. L., Daffer, W. H., Zawodny, J. M., Bernath, P. F., Hopfel, K. W., Walker, K. A., Knosp, B. W., Boone, C., Remsberg, E. E., Santee, M. L., Harvey, V. L., Pawson, S., Jackson, D. R., Deaver, L., McElroy, C. T., McLinden, C. A., Drummond, J. R., Pumphrey, H. C., Lambert, A., Schwartz, M. J., Froidevaux, L., McLeod, S., Takacs, L. L., Suarez, M. J., Trepte, C. R., Cuddy, D. C., Livesey, N. J., Harwood, R. S., and Waters, J. W.: Solar occultation satellite data and derived meteorological products: sampling issues and comparisons with Aura Microwave Limb Sounder, *J. Geophys. Res.*, 112, D24S50, doi:10.1029/2007JD008709, 2007.
- Manney, G. L., Schwartz, M. J., Krüger, K., Santee, M. L., Pawson, S., Lee, J. N., Daffer, W. H., Fuller, R. A., and Livesey, N. J.: Aura Microwave Limb Sounder observations of dynamics and transport during the record-breaking 2009 Arctic stratospheric major warming, *Geophys. Res. Lett.*, 36, L12815, doi:10.1029/2009GL038586, 2009.
- Manney, G. L., Santee, M. L., Rex, M., Livesey, N. J., Pitts, M. C., Veefkind, P., Nash, E. R., Wohltmann, I., Lehmann, R., Froidevaux, L., Poole, L. R., Schoeberl, M. R., Haffner, D. P., Davies, J., Dorokhov, V., Gernandt, H., Johnson, B., Kivi, R., Kyro, E., Larsen, N., Levelt, P. F., Makshtas, A., McElroy, C. T., Nakajima, H., Parrondo, M. C., Tarasick, D. W., von der Gathen, P., Walker, K. A., and Zinoviev, N. S.: Unprecedented Arctic Ozone loss in 2011, *Nature*, 478, 469–475, doi:10.1038/nature10556, 2011.
- Manney, G. L., Lawrence, Z. D., Santee, M. L., Read, W. G., Livesey, N. J., Lambert, A., Froidevaux, L., Pumphrey, H. C., and Schwartz, M. J.: A minor sudden stratospheric warming with a major impact: Transport and polar processing in the 2014/2015 Arctic winter, *Geophys. Res. Lett.*, 42, 7808–7816, doi:10.1002/2015GL065864, 2015.
- Marquardt, D.: An algorithm for least squares estimation on nonlinear parameters, *J. Soc. Ind. Appl. Math.*, 11, 431–41, 1963.
- McLandress, C., Scinocca, J. F., Shepherd, T. G., Reader, M. C., and Manney, G. L.: Dynamical Control of the Mesosphere by Orographic and Nonorographic Gravity Wave Drag during the Extended Northern Winters of 2006 and 2009, *J. Atmos. Sci.*, 70, 2152–2169, doi:10.1175/JAS-D-12-0297.1, 2013.
- Minschwaner, K., Manney, G. L., Livesey, N. J., Pumphrey, H. C., Pickett, H. M., Froidevaux, L., Lambert, A., Schwartz, M. J., Bernath, P. F., and Walker, K. A.: The photochemistry of carbon monoxide in the stratosphere and mesosphere evaluated from observations by the Microwave Limb Sounder on the Aura satellite, *J. Geophys. Res.*, 115, D13303, doi:10.1029/2009JD012654, 2010.
- Muscari, G., di Sarra, A. G., de Zafra, R. L., Lucci, F., Baordo, F., Angelini, F., and Fiocco, G.: Middle atmospheric O₃, CO, N₂O, HNO₃, and temperature profiles during the warm Arctic winter 2001–2002, *J. Geophys. Res.*, 112, D14304, doi:10.1029/2006JD007849, 2007.
- Nedoluha, G. E., Gomez, R. M., Neal, H., Lambert, A., Hurst, D., Boone, C., and Stiller, G.: Validation of long-term measurements of water vapor from the midstratosphere to the mesosphere at two Network for the Detection of Atmospheric Composition Change sites, *J. Geophys. Res.-Atmos.*, 118, 934–942, doi:10.1029/2012JD018900, 2013.
- Nedoluha, G. E., Connor, B. J., Mooney, T., Barrett, J. W., Parrish, A., Gomez, R. M., Boyd, I., Allen, D. R., Kotkamp, M., Kremser, S., Deshler, T., Newman, P., and Santee, M. L.: 20 years of ClO measurements in the Antarctic lower stratosphere, *Atmos. Chem. Phys.*, 16, 10725–10734, doi:10.5194/acp-16-10725-2016, 2016.
- Ohyama, H., Nagahama, T., Mizuno, A., Nakane, H., and Ogawa, H.: Observations of stratospheric and mesospheric O₃ with a millimeter-wave radiometer at Rikubetsu, Japan, *Earth Planets Space*, 68, 34, doi:10.1186/s40623-016-0406-4, 2016.
- Palm, M., Hoffmann, C. G., Golchert, S. H. W., and Notholt, J.: The ground-based MW radiometer OZORAM on Spitsbergen – description and status of stratospheric and mesospheric O₃-measurements, *Atmos. Meas. Tech.*, 3, 1533–1545, doi:10.5194/amt-3-1533-2010, 2010.
- Pumphrey, H. C., Filipiak, M. J., Livesey, N. J., Schwartz, M. J., Boone, C., Walker, K. A., Bernath, P., Ricaud, P., Barret, B., Clerbaux, C., Jarnot, R. F., Manney, G. L., and Waters,

- J. W.: Validation of middle-atmosphere carbon monoxide retrievals from MLS on Aura, *J. Geophys. Res.*, 112, D24S38, doi:10.1029/2007JD008723, 2007.
- Picone, J. M., Hedin, A. E., Drob, D. P., and Aikin, A. C.: NRLMSISE-00 empirical model of the atmosphere: Statistical comparisons and scientific issues, *J. Geophys. Res.*, 107, 1468, doi:10.1029/2002JA009430, 2002.
- Raffalski, U., Berg, H., Hochschild, G., and Kopp, G.: Continuous ozone measurements over Kiruna during winter/spring 2002: A new millimeter wave radiometer operated at the Swedish Institute of Space Physics, Kiruna, Sweden, Proceedings of the Sixth European Symposium on Stratospheric Ozone Research, Gothenberg, Sweden, 369–372, 2002.
- Rienecker, M. M., Suarez, M. J., Gelaro, R., Todling, R., Bacmeister, J., Liu, E., Bosilovich, M. G., Schubert, S. D., Takacs, L., Kim, G.-K., Bloom, S., Chen, J., Collins, D., Conaty, A., da Silva, A., Gu, W., Joiner, J., Koster, R. D., Lucchesi, R., Molod, A., Owens, T., Pawson, S., Pegion, P., Redder, C. R., Reichle, R., Robertson, F. R., Ruddick, A. G., Sienkiewicz, M., and Woollen, J.: MERRA: NASA's Modern-Era Retrospective Analysis for Research and Applications, *J. Climate*, 24, 3624–3648, doi:10.1175/JCLI-D-11-00015.1, 2011.
- Rodgers, C. D. and Connor, B. J.: Intercomparison of remote sounding instruments, *J. Geophys. Res.*, 108, 4116, doi:10.1029/2002JD002299, 2003.
- Rogers, C. D.: Inverse methods for atmospheric remote sounding: Theory and practice, in: Series on atmospheric and ocean physics, Volume 2, World Scientific, Singapore, 2000.
- Rosenkranz, P. W.: Absorption of microwaves by atmospheric gases, in: Atmospheric remote sensing by microwave radiometry, edited by: Janssen, M. A.: Wiley, New York, 37–90, 1993.
- Rosenkranz, P. W.: Water vapor microwave continuum absorption: A comparison of measurements and models, *Radio Sci.*, 33, 919–928, 1998.
- Rothman, L. S., Gordon, I. E., Barbe, A., Chris Benner, D., Bernath, P. F., Birk, M., Boudon, V., Brown, L. R., Campargue, A., Champion, J.-P., Chance, K., Couderti, L. H., Dana, V., Devi, V. M., Fally, S., Flaud, J.-M., Gamache, R. R., Goldman, A., Jacquemart, D., Kleiner, I., Lacome, N., Lafferty, W. J., Mandin, J.-Y., Massie, S. T., Mikhailenko, S. N., Miller, C. E., Moazzen-Ahmadi, N., Naumenko, O. V., Nikitin, A. V., Orphal, J., Perevalov, V. I., Perrin, A., Predoi-Cross, A., Rinsland, C. P., Rotger, M., Simeckova, M., Smith M. A. H., Sung, K., Tashkun, S. A., Tennyson, J., Toth, R. A., Vandaele, A. C., and Vander Auwera, J.: The HITRAN 2008 molecular spectroscopic database, *J. Quant. Spectrosc. Ra.*, 110, 533–572, 2009.
- Ryan, N. J. and Walker, K. A.: The effect of spectroscopic parameter inaccuracies on ground-based millimeter wave remote sensing of the atmosphere, *J. Quant. Spectrosc. Ra.*, 161, 50–59, doi:10.1016/j.jqsrt.2015.03.012, 2015.
- Schwartz, M., Pumphrey, H., Livesey, N., and Read, W.: MLS/Aura Level 2 Carbon Monoxide (CO) Mixing Ratio V004, version 004, Greenbelt, MD, USA, Goddard Earth Sciences Data and Information Services Center (GES DISC), available at: doi:10.5067/AURA/MLS/DATA2005, last access: January 2016, 2015.
- Solomon, S., Garcia, R. R., Olivero, J. G., Bevilacqua, R. M., Schwartz, P. R., Clancy, R. T., and Muhleman, D. O.: Photochemistry and Transport of Carbon Monoxide in the Middle Atmosphere, *J. Atmos. Sci.*, 42, 1072–1083, 1985.
- Straub, C., Espy, P. J., Hibbins, R. E., and Newnham, D. A.: Mesospheric CO above Troll station, Antarctica observed by a ground based microwave radiometer, *Earth Syst. Sci. Data*, 5, 199–208, doi:10.5194/essd-5-199-2013, 2013.
- Swadely, S. D., Poe, G. A., Bell, W., Hong, Y., Kunkee, D. B., McDermid, I. S., and Leblanc, T.: Analysis and Characterization of the SSMIS Upper Atmosphere Sounding Channel Measurements, *IEEE T. Geosci. Remote.*, 46, 962–983, 2008.
- Waters, J., Froidevaux, L., Harwood, R., Jarno, R., Pickett, H., Read, W., Siegel, P., Cofield, R., Filipiak, M., Flower, D., Holden, J., Lau, G., Livesey, N., Manney, G., Pumphrey, H., Santee, M., Wu, D., Cuddy, D., Lay, R., Loo, M., Perun, V., Schwartz, M., Stek, P., Thurstans, R., Boyles, M., Chandra, S., Chavez, M., Chen, G.-S., Chudasama, B., Dodge, R., Fuller, R., Girard, M., Jiang, J., Jiang, Y., Knosp, B., LaBelle, R., Lam, J., Lee, K., Miller, D., Oswald, J., Patel, N., Pukala, D., Quintero, O., Scaff, D., Snyder, W., Tope, M., Wagner, P., and Walch, M.: The Earth Observing System Microwave Limb Sounder (EOSMLS) on the Aura satellite, *IEEE T. Geosci. Remote.*, 44, 1075–1092, 2006.
- York, D., Evensen, N. M., Martinez, M. L., and Delgado, J. D. B.: Unified equations for the slope, intercept, and standard errors of the best straight line, *Am. J. Phys.*, 72, 367–375, 2004.